Mod Rheumatol (2009) 19:180–186
DOI 10.1007/s10165-008-0147-8

ORIGINAL ARTICLE

Treatment of juxta-articular intraosseous cystic lesions in rheumatoid arthritis patients with interconnected porous calcium hydroxyapatite ceramic

Kohji Kuriyama · Jun Hashimoto · Tsuyoshi Murase · Masakazu Fujii · Akihide Nampei · Makoto Hirao · Hideki Tsuboi · Akira Myoui · Hideki Yoshikawa

Received: 16 June 2008 / Accepted: 18 November 2008 / Published online: 27 January 2009

Abstract In patients with rheumatoid arthritis (RA), juxta-articular intraosseous cystic lesions may cause spontaneous pathological fractures. The outcome of curettage and the packing of such lesions with interconnected porous calcium hydroxyapatite ceramic (IP-CHA) was investigated. Twelve lesions were treated in ten RA patients (three men and seven women with a mean age of 59 years). Ten lesions were associated with impending pathological fracture involving the articular surface. In all patients, curettage and packing of the bone cavity with IP-CHA were done. Assessment was based on final radiographs obtained an average of 30 months after surgery (range 10–47 months). Absorption of the implanted IP-CHA, expansion of the lesion, implant incorporation into host bone, and postoperative fractures were investigated. At final follow-up, there was no absorption of the implanted IP-CHA in any of the lesions. Expansion of the radiolucent area was only noted in one lesion. Seven of the other 11 lesions showed major incorporation of IP-CHA into host bone, while minor incorporation was seen in four lesions. There were no postoperative fractures. In conclusion, curettage and packing with IP-CHA is a feasible method of preventing pathological fracture due to juxta-articular intraosseous cystic lesions in RA patients.

Keywords Interconnected porous calcium hydroxyapatite ceramic · Juxta-articular intraosseous cystic lesions · Rheumatoid arthritis · Surgical treatment

Electronic supplementary material The online version of this article (doi:10.1007/s10165-008-0147-8) contains supplementary material, which is available to authorized users.

K. Kuriyama
Department of Orthopaedic Surgery,
Toyonaka Municipal Hospital, Toyonaka, Japan

J. Hashimoto (✉) · T. Murase · A. Nampei · M. Hirao · A. Myoui · H. Yoshikawa
Department of Orthopaedic Surgery,
Osaka University Graduate School of Medicine,
2-2 Yamadaoka, Suita 565-0871, Japan
e-mail: junha@ort.med.osaka-u.ac.jp

M. Fujii
Department of Orthopaedic Surgery,
Gratia Hospital, Minoh, Japan

H. Tsuboi
Department of Orthopaedic Surgery,
Osaka Rosai Hospital, Sakai, Japan

Introduction

Juxta-articular intraosseous cystic lesions in patients with rheumatoid arthritis (RA) have been variously termed synovial cysts [1], subchondral cysts [2], subarticular pseudocysts [3], or geodes [4]. These lesions are often found during the course of RA, but aggressive surgical treatment is not usually performed because the patient has no symptoms unless spontaneous or traumatic intra-articular fracture occurs. Once fracture occurs, however, joint destruction progresses rapidly due to mechanical stress rather than disease-related inflammation, and daily activities can be severely affected [5–8]. It is important to maintain the subchondral bone of RA patients in good condition, not only to prevent pathological fractures but also because of the possible need to perform arthroplasty in the future.

We have treated juxta-articular intraosseous cystic lesions in RA patients by curettage and packing with a hydroxyapatite filler (interconnected porous calcium hydroxyapatite ceramic, IP-CHA) in order to prevent subchondral fractures. In our experience, IP-CHA undergoes

extensive incorporation into host bone more rapidly than other types of porous calcium hydroxyapatite ceramic [9]. The purpose of the present study was to evaluate the preliminary results obtained with this treatment.

Materials and methods

Between September 2003 and March 2005, we treated 12 juxta-articular cystic lesions in ten RA patients (Table 1). Ten of the 12 lesions were associated with a risk of impending intra-articular fracture, judging from the fragile appearance of the subchondral bone on radiographs. The other two lesions were treated as an additional procedure during synovectomy and matched ulnar resection, respectively. All patients fulfilled the American Rheumatism Association diagnostic criteria for RA [10]. Three patients were men and seven were women, with an average age of 59 years (range 49–72 years) at the time of operation. The location and size of the lesions were determined by examination of preoperative anteroposterior plain X-ray films. Eight lesions were located in the distal radius (four involved most of the subarticular surface, two were located in the radial styloid process, and the remaining two were at the center of the subarticular bone), while one lesion was located in the head of the ulna, one in the center of the proximal tibial condyle, one in the medial malleolus of the tibia, and the lateral malleolus of the fibula. The lesions were classified into three groups on the basis of the transverse diameter: large lesions had a diameter of greater than two-thirds of the articular surface ($n = 6$), medium lesions had a diameter of one-third to two-thirds of the articular surface ($n = 4$), and small lesions had a diameter of less than one-third ($n = 2$). Disease activity was assessed preoperatively from the C-reactive protein (CRP) level and the tenderness and swelling of the involved joint. The Steinbrocker functional class and stage [11] and the Larsen grade [12] of the joint were also assessed. Each patient's medications were recorded (Table 2).

Operative technique

Surgery was performed under regional or general anesthesia. A pneumatic tourniquet was applied. Under fluoroscopic guidance as needed, each juxta-articular lesion was exposed via an extra-articular approach. For lesions of the distal radius, the second or fourth extensor retinaculum was opened through a dorsal skin incision about 2–3 cm long. For lesions of the knee, ankle, and ulna, a skin incision was made just over the target. A small window (about 8 mm square) was made in the wall of the lesion, taking care to preserve the periosteum of the resected bone. After performing intralesional curettage and complete resection of the capsule of the cyst, the residual bone defect was filled with blocks and granules of sterilized IP-CHA (Stryker Co., Tokyo, Japan). Then the small bone section was replaced in order to close the cortical window. After surgery, a splint was not applied and range-of-movement exercises were commenced immediately. Together with the above procedure, synovectomy of the wrist and knee joint was also done in two patients who had wrist synovitis (case 2) and a huge synovial cyst (case 9), respectively. Matched ulnar head resection was also performed in one patient (case 5) who presented with disability of the distal radioulnar joint.

Table 1 Details of the 12 lesions

Case no.	Age	Gender	Location	Size (mm)	Follow-up (months)	Expansion	Absorption	Incorporation (grade)	Combined operation
1	55	M	R distal radius	35 × 20 (large)	42	–	–	2	
			L distal radius	35 × 12 (large)		–	–	3	
			Distal ulna	16 × 9 (large)		–	–	3	
2	52	F	Proximal tibia	50 × 32 (medium)	10	–	–	2	#1
3	61	F	Distal fibula	33 × 21 (large)	40	–	–	3	
4	53	F	Distal radius	19 × 15 (medium)	47	–	–	3	
5	72	F	Distal radius	11 × 10 (small)	22	–	–	3	#2
6	63	M	Distal radius	25 × 12 (medium)	37	–	–	3	
7	49	F	Distal radius	35 × 20 (large)	16	+	–	–	
8	59	M	Distal radius	16 × 9 (medium)	19	–	–	2	
9	55	F	Distal radius	7 × 4 (small)	36	–	–	3	#1
10	71	F	Distal tibia	29 × 17 (large)	29	–	–	2	

Expansion expansion of the radiolucent area, *Absorption* absorption of implanted IP-CHA, *Combined operation* other procedures performed simultaneously, *#1* synovectomy, *#2* matched ulnar resection

Table 2 Details of the ten patients

Case no.	Preoperative CRP (mg/dl)	Location	Class	Stage	Larsen grade	Local tenderness	Local swelling	Medications (daily doses except for MTX)
1	0.9	R distal radius	3	4	4	Mild	Mild	Predonine 10 mg, MTX 6 mg
		L distal radius			4	Mild	Mild	
		Distal ulna			4	Mild	Mild	
2	2.9	Proximal tibia	2	3	2	Moderate	Severe	Predonine 10 mg, MTX 6 mg, bucillamine 300 mg
3	0.2	Distal fibula	2	3	4	Non	Non	MTX 4 mg, metronidazole, salazosulfapyridine 1,000 mg
4	0.2	Distal radius	2	3	4	Mild	Mild	Predonine 7.5 mg, MTX 6 mg
5	1.3	Distal radius	3	2	4	Moderate	Moderate	Predonine 5 mg, salazosulfapyridine 1,000 mg
6	0.9	Distal radius	2	3	3	Mild	Moderate	Predonine 5 mg, bucillamine 200 mg
7	2.5	Distal radius	3	3	5	Moderate	Moderate	Predonine 10 mg
8	0.8	Distal radius	2	3	5	Mild	Mild	Salazosulfapyridine 1,000 mg
9	0.4	Distal radius	1	2	3	Moderate	Moderate	Predonine 1 mg, salazosulfapyridine 1,000 mg
10	1.2	Distal tibia	2	4	2	Non	Non	Salazosulfapyridine 1,000 mg

Class Steinbrocker functional class, *Stage* Steinbrocker stage, *MTX* methotrexate (weekly doses)

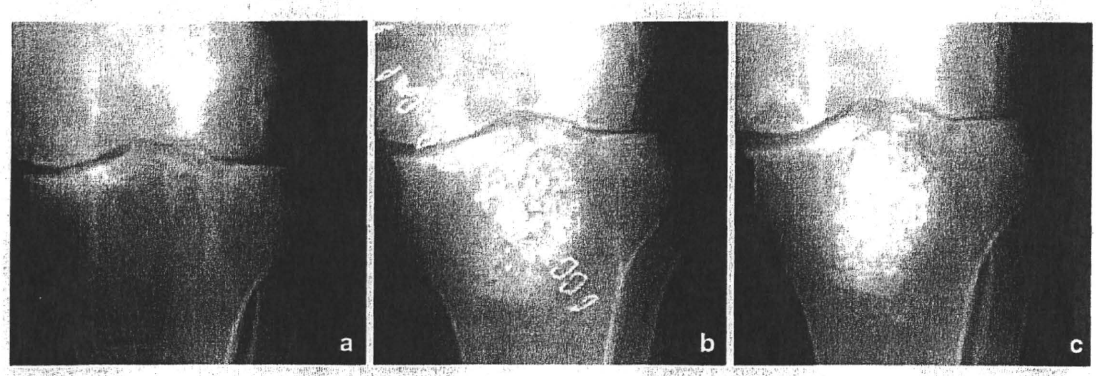

Fig. 1 Case 2: **a** preoperative radiograph reveals a large radiolucent area in the proximal tibia. **b** Radiograph obtained just after surgery. **c** At 10 months after surgery, there is no absorption of IP-CHA or expansion of the cystic lesion

Radiological assessment

Radiological assessment was performed by comparing radiographs obtained just after surgery with those obtained at final follow-up at an average of 30 months (range 10–47 months). The following four points were assessed: absorption of the implanted IP-CHA, expansion of the cystic lesion, incorporation of the implanted IP-CHA into host bone, and occurrence of postoperative fracture. The extent of incorporation of the implanted IP-CHA by host bone was graded according to the previously reported method [9]. In brief, Grade 1 was no incorporation, Grade 2 was minor incorporation (a slight increase in the density of the implanted IP-CHA granules and partial disappearance of the radiolucent lines between implant and host bone), and Grade 3 was major incorporation (a marked increase of density and/or disappearance of the spaces between IP-CHA granules).

Clinical assessment

Complications such as fracture, infection, and joint contracture related to surgery were assessed by clinical review.

Results

Absorption of the implanted IP-CHA did not occur in any patient and there were no postoperative fractures. Eleven of the 12 lesions showed no expansion at final follow-up. In these 11 lesions, the density of the implanted IP-CHA increased over time, and the granules appeared to become fused and incorporated into the surrounding host bone. Four of the 11 lesions showed grade 2 incorporation and seven lesions showed grade 3 incorporation at final follow-up (Figs. 1, 2). One patient (case 7) had poorly controlled RA due to concomitant hepatic and pancreatic dysfunction,

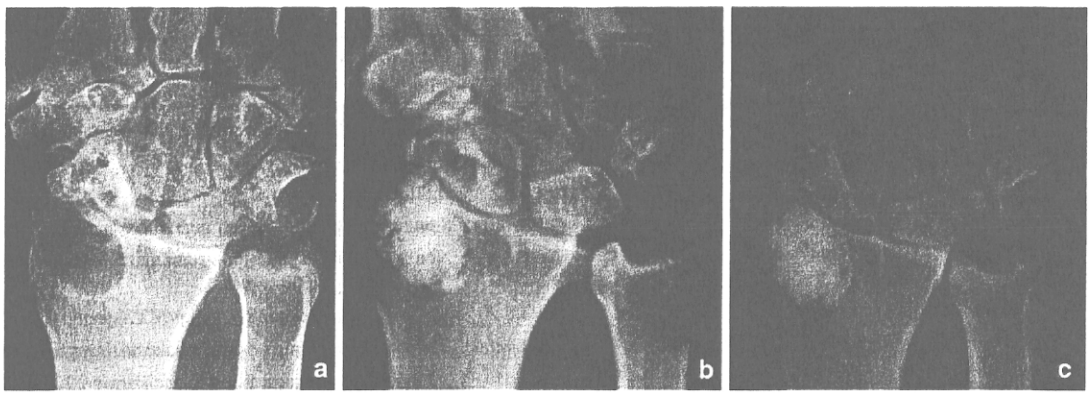

Fig. 2 Case 6: **a** preoperative radiograph reveals a large radiolucent area in the distal radius. **b** Appearance just after surgery. **c** At 37 months after surgery, there is no absorption of IP-CHA or expansion of the cystic lesion

Fig. 3 Case 7: **a** preoperative radiograph reveals a large radiolucent area in the distal radius. **b** Appearance just after the operation. Curettage and IP-CHA implantation are inadequate. **c** At 16 months after surgery, there is expansion of the cystic lesion, but no reabsorption of implanted IP-CHA

and expansion of the cystic lesion occurred with appearance of a radiolucent zone around the implanted IP-CHA at final follow-up (Fig. 3).

Before surgery, cases 5 and 9 had pain and swelling of the wrist. Their pain and swelling improved after synovectomy in addition to curettage and packing of the lesions. In case 2 (Fig. 1), preoperative knee joint pain was improved after curettage of a tibial cystic lesion and packing with IP-CHA, as well as synovectomy of the knee joint. The range of joint motion did not change significantly after surgery. There were no complications related to implanting IP-CHA, such as excessive postoperative drainage, erythema, or wound infection.

Discussion

Juxta-articular intraosseous cystic lesions are commonly found during the course of RA, and these lesions can cause spontaneous pathological fractures that result in extensive joint destruction [5–8]. Nakagawa et al. reported two cases of giant geodes involving the olecranon process. They performed surgery for an associated pathological fracture in one patient and treated the other patient prophylactically with an autologous iliac bone graft to prevent fracture [5]. Lowthian et al. reported a patient who had multiple pathological fractures of the phalanges due to cystic lesions that led to residual instability of the

fingers despite surgical treatment [6]. Wordsworth et al. reported a patient with a pathological fracture of the proximal ulna that was initially treated conservatively but failed to unite, so that bone grafting was subsequently performed [7]. Rappoport et al. reported three patients with chronic RA who developed pathological fractures of the olecranon process due to erosions or cysts [8]. Although intraosseous cystic lesions often occur in patients with active RA and wrist joint involvement, it is difficult to detect such lesions associated with fracture of the distal radius by either clinical or radiographic assessment. One reason might be that intermittent radiological evaluation does not allow detection of pathological fracture of the subchondral bone associated with an intraosseous cystic lesion. The second reason might be that concomitant pathological changes, including erosions, destruction of cartilage, and subluxation of the radiocarpal joint, make it difficult to detect an intraosseous cystic lesion associated with fracture of the distal radius. In one of our patients, joint collapse was associated with the cystic lesion on radiographs. Figure 4a shows a double contour indicating a fracture adjacent to this patient's intraosseous cystic lesion, while Fig. 4b displays rapid progression of joint destruction after six months. Once joint destruction has occurred (as in Fig. 4b), it is quite difficult to detect the presence of a cystic lesion near the radiocarpal joint. The findings in this patient suggest that prophylactic surgical treatment of juxta-articular intraosseous cystic lesions in RA patients could be useful to prevent impending fracture, as is the case with benign bone tumors like solitary bone cyst or giant cell tumor of bone. However, surgery is not often performed in RA patients for the following reasons (among others). First, a juxta-articular intraosseous cystic lesion causes no symptoms or inconvenience itself. Second, autologous bone grafting is associated with donor site morbidity [13], and there are limitations on grafting because of the possible need for multiple operations in patients with RA. Third, an artificial bone substitute with excellent bone conduction properties was not available in the past. Conventional hydroxyapatite implants achieve little bone ingrowth into the deeper regions because there are few interpore connections allowing bone marrow cells to infiltrate into the implant, so a hydroxyapatite implant does not gain sufficient mechanical strength. On the other hand, IP-CHA has demonstrated excellent osteoconductivity in animal models as well as in clinical trials [9, 14]. IP-CHA has a high porosity (75%), and the pores show uniform connections with each other like the pores in cancellous bone. The majority of the pores are approximately 100–200 μm in diameter with interconnections that are about 40 μm in diameter, and the compression strength of IP-CHA is about 10 MPa [14]. These structural differences from conventional hydroxyapatite confer excellent bone conduction, so that host bone ingrowth is sufficient to achieve adequate mechanical strength without autologous bone grafting. On the other hand, Suzuki et al. reported a patient with a giant geode in the tibial condyle that was successfully treated with calcium phosphate cement (CPC) [15]. Although the use of CPC provides initial high mechanical strength and incorporation of the implant surface into host bone may occur, a CPC block has no pores. IP-CHA provides sufficient mechanical strength after new bone ingrowth occurs due to its cancellous

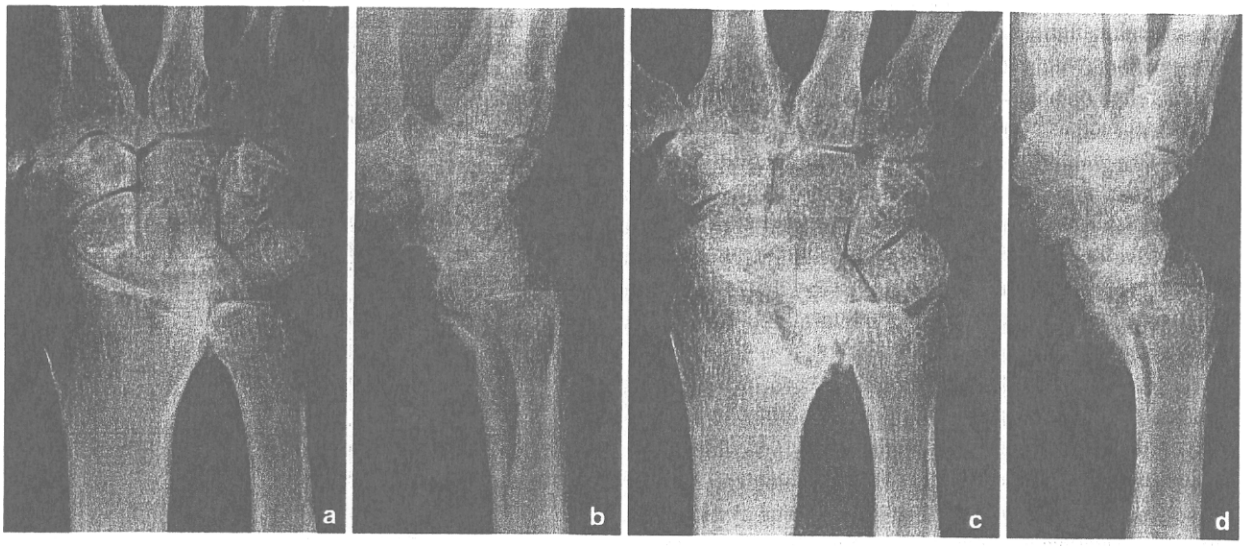

Fig. 4 A 54-year-old man: **a, b** there is a pathological fracture and cystic lesion of the lunate fossa in the distal radius. **c, d** After 6 months, joint destruction shows marked progression

structure, and it might also show more physiological resistance to mechanical stress. We aimed to utilize these properties of IP-CHA to improve mechanical strength in the treatment of intraosseous cystic lesions, and achieved good radiological results in the present series. We also found that IP-CHA is easy to handle and there is little risk of leakage into adjacent joints.

In patients with RA, the bone adjacent to involved joints develops juxta-articular osteoporosis, erosions, and intraosseous cystic lesions, with these changes being considered to be due to an increase of osteoclastic bone resorption [16–19] secondary to local overproduction of bone-resorbing cytokines. The present study revealed that IP-CHA was resistant to absorption, even in the pathological state of RA for at least 47 months after surgery. This property of IP-CHA makes it suitable for treating RA because a more biodegradable material could also be remodeled into bone but might then be affected by juxta-articular osteoporosis or erosive changes.

One of our patients had severe RA that could not be controlled due to concomitant hepatic and pancreatic dysfunction. The CRP level of this patient remained above 2.0 mg/dl before and after surgery, and expansion of the cystic lesion occurred despite surgical treatment. This case suggests that curettage and implantation of IP-CHA will not suppress local disease activity and prevent the expansion of a lesion if the patient has poorly controlled RA. Recent advances in the treatment of RA with the advent of biological agents have made it possible to prevent the progression of joint destruction [20, 21]. Accordingly, the expansion of cystic lesions may also be prevented by controlling disease activity with more effective drugs. Such advances in medical therapy may allow curettage and packing with IP-CHA to become a better treatment for juxta-articular intraosseous cystic lesions.

In patients with RA, the goals of surgical treatment include relief of pain and improvement of joint function. Procedures such as synovectomy, arthrodesis, and resection arthroplasty mainly target pain relief. Implant arthroplasty targets both pain relief and functional improvement, while tendon transfer and tendon grafting are procedures that aim to improve function. The present procedure represents a new category of surgical treatment for RA that is indicated to prevent impending articular fracture due to a large intraosseous cystic lesion.

In RA patients, joint destruction is a process that involves several events, including destruction of the surface cartilage, resorption of mineralized cartilage, and erosion of subchondral bone [22]. Pathological fracture associated with a juxta-articular intraosseous cystic lesion can also contribute to joint destruction, but not all cystic lesions will cause fractures. The size and location of a lesion, as well as juxta-articular osteoporosis, marginal sclerosis, systemic disease activity, and the local inflammatory response might all influence the risk of fracture. To adequately decide the indications for this procedure, a method for assessing the risk of impending fracture associated with juxta-articular intraosseous cystic lesions is the next issue to be clarified. Recently, we have been evaluating the impending fracture with CT, which shows the size, location and features of a lesion clearly (see Fig. 1 in the "Electronic supplementary material"). Limitations of the present study include the small number of subjects and the lack of a control group. However, these preliminary results are still encouraging and suggest that treatment with IP-CHA may become a useful method for preventing fracture associated with juxta-articular intraosseous cystic lesions in RA patients.

Conflict of interest statement The authors declare that there are no competing financial interests.

References

1. Crane AR, Scarano JT. Synovial cysts (ganglia) of bone. J Bone Joint Surg Am. 1967;49:355–61.
2. Harrison MHM, Schajowicz F, Trueta J. Osteoarthritis of the hip and study of the nature and evolution of the disease. J Bone Joint Surg Br. 1953;35:598–626.
3. Cruickshank B, Macleod IG, Shearer WS. Subarticular pseudocysts in rheumatoid arthritis. J Fac Radiol. 1954;5:218–26.
4. Resnick D, Niwayama G, Coutts RD. Subchondral cysts (geodes) in arthritic disorders: pathologic and radiographic appearance of the hip joint. Am J Roentgenol. 1977;128:799–806.
5. Nakagawa N, Abe S, Saegusa Y, Kimura H, Imura S, Nishibayashi Y, et al. Giant geode at the olecranon in the rheumatoid elbow—two case reports. Clin Rheumatol. 2004;23:358–61.
6. Lowthian PJ, Calin A. Geode development and multiple fractures in rheumatoid arthritis. Ann Rheum Dis. 1985;44:130–3.
7. Wordsworth BP, Mowat AG, Watson NA. Fracture through a geode in the proximal ulna. Br J Rheumatol. 1984;23:110–2.
8. Rappoport AS, Sosman JL, Weissman BN. Spontaneous fractures of the olecranon process in rheumatoid arthritis. Radiology. 1976;119:83–4.
9. Myoui A, Tamai N, Nishikawa M, Yoshikawa H, Araki N, Nakase T, et al. Three-dimensionally engineered hydroxyapatite ceramics with interconnected pores as a bone substitute and tissue engineering scaffold. Biomater Orthop. 2003;13:287–300.
10. Arnett FC, Edworthy SM, Bloch DA, McShane DJ, Fries JF, Cooper NS, et al. The American Rheumatism Association 1987 revised criteria for the classification of rheumatoid arthritis. Arthritis Rheum. 1988;31:315–24.
11. Steinbrocker O, Traeger GH, Batterman RC. Therapeutic criteria in rheumatoid arthritis. J Am Med Assoc. 1949;140:659–62.
12. Larsen A, Dale K, Eek M. Radiographic evaluation of rheumatoid arthritis and related conditions by standard reference films. Acta Radiol Diagn. 1977;18:481–91.
13. Goulet JA, Senunas LE, DeSilva GL, Greenfield ML. Autogenous iliac crest bone graft. Complications and functional assessment. Clin Orthop Relat Res. 1997;339:76–81.
14. Tamai N, Myoui A, Tomita T, Nakase T, Tanaka J, Ochi T, et al. Novel hydroxyapatite ceramics with an interconnective porous

structure exhibit superior osteoconduction in vivo. J Biomed Mater Res. 2002;59:110–7.
15. Suzuki M, Kim T, Tamai H, Fujiyoshi T, Moriya H. Giant geode treated with calcium phosphate cement in a rheumatoid knee. J Rheumatol. 2005;32:1846–8.
16. Bromley M, Woolley DE. Chondroclasts and osteoclasts at subchondral sites of erosion in the rheumatoid joint. Arthritis Rheum. 1984;27:968–75.
17. Gravallese EM, Harada Y, Wang JT, Gorn AH, Thornhill TS, Goldring SR. Identification of cell types responsible for bone resorption in rheumatoid arthritis and juvenile rheumatoid arthritis. Am J Pathol. 1998;152:943–51.
18. Kong YY, Feige U, Sarosi I, Bolon B, Tafuri A, Morony S, et al. Activated T cells regulate bone loss and joint destruction in adjuvant arthritis through osteoprotegerin ligand. Nature. 1999;402:304–9.
19. Gravallese EM, Manning C, Tsay A, Naito A, Pan C, Amento E, et al. Synovial tissue in rheumatoid arthritis is a source of osteoclast differentiation factor. Arthritis Rheum. 2000;43:250–8.
20. van der Heijde D, Landewe R, Klareskog L, Rodriguez-Valverde V, Settas L, Pedersen R, et al. Presentation and analysis of data on radiographic outcome in clinical trials: experience from the TEMPO study. Arthritis Rheum. 2005;52:49–60.
21. Genovese MC, Bathon JM, Fleischmann RM, Moreland LW, Martin RW, Whitmore JB, et al. Long-term safety, efficacy, and radiographic outcome with etanercept treatment in patients with early rheumatoid arthritis. J Rheumatol. 2005;32:1232–42.
22. Schett G. Erosive arthritis. Arthritis Res Ther. 2007;9(Suppl 1):S2.

Rheumatology 2009;48:643–649
Advance Access publication 27 April 2009

doi:10.1093/rheumatology/kep044

Equivalent osteoblastic differentiation function of human mesenchymal stem cells from rheumatoid arthritis in comparison with osteoarthritis

Daiki Morimoto[1], Shoko Kuroda[2], Takuji Kizawa[1], Koji Nomura[1], Chikahisa Higuchi[1], Hideki Yoshikawa[1] and Tetsuya Tomita[1]

Objective. To evaluate the osteoblastic differentiation of human mesenchymal stem cells (hMSCs) in patients with RA.
Methods. Heparinized bone marrow aspirate was obtained from patients with OA and RA. Mononuclear cells were cultured for 2 weeks and a colony-forming assay was performed. The phenotype of cells was analysed by flow cytometry. Passage 2 cells were cultured with β-glycerophosphate (bGP) in the control group and bGP, ascorbic acid and dexamethasone in the differentiation group. After 2 weeks, ALP staining and activity were performed. After 3 weeks, Alizarin Red S assay was performed. Total RNA was extracted from cells cultured for 2 and 3 weeks. Gene expression of bone formation factor was examined by real-time PCR.
Results. The phenotype of cells was identical in both OA and RA and the content was thought to be hMSCs. The results of ALP activity and Alizarin Red S assay showed higher levels in the differentiation group for both OA and RA samples compared with the control group. The results of a colony-forming assay were identical in both OA and RA samples. Gene expression in the differentiation group was higher than in the control group in both OA and RA samples. There was no significant difference between OA and RA samples in all experiments.
Conclusion. The function of osteoblastic differentiation of hMSCs is similar between OA and RA.

KEY WORDS: Rheumatoid arthritis, Human meschenchymal stem cells, Osteoblast, Bone formation.

Introduction

RA is a chronic inflammatory disease that shows diffuse symmetrical polyarthritis [1]. In RA, progressive joint destruction and general osteoporosis are the characteristic symptoms [2, 3] and patients with RA have a higher risk of fracture [4–6]. Although the aetiology of RA has not been clearly elucidated, it is demonstrated that inflammatory cytokines such as IL-1 and TNF-α and the activation of osteoclasts play an important role in RA [7–10]. In normal bone mineral tissue, bone metabolism is preserved between bone resorption and formation [11–13]. In RA, bone resorption is accelerated and unbalanced with bone formation [14] and although the mechanism of bone resorption by osteoclasts has been evaluated, bone formation has been rarely evaluated, and it remains unclear whether bone formation is accelerated, not changed or attenuated. In previous studies, bone metabolism in patients with RA was evaluated by measuring the biomarkers of serum and urine, and the results suggested that bone resorption was accelerated and bone formation was attenuated in RA [15, 16]. However, in these studies, bone formation was evaluated indirectly.

Bone formation is mainly controlled by the function of osteoblasts. Osteoblasts are differentiated from human mesenchymal stem cells (hMSCs) [17] and it is suggested that hMSCs differentiate into osteoblastic cells followed by the stages of production of bone matrix protein and mineralization [18].

In this study, we obtained hMSCs from patients with OA and RA and evaluated the capability of osteoblastic differentiation of hMSCs.

Patients and methods

Patients

All patients in the present study comprised women. In patients with OA, 26 samples were examined and mean patient age was 73.2 years (range 60–83 years); in patients with RA, 20 samples were examined and mean patient age was 58.9 years (range 46–81 years). Patients with RA who had been previously treated with biologics were excluded. Clinical and demographic features of patients with RA are shown in Table 1.

All patients with RA satisfied the 1987 ACR revised diagnostic criteria [19]. All patients with OA were assessed with radiographic images according to the Kellgren and Lawrence classification [20]. All patients with OA satisfied grade III or IV. The written informed consent from all patients was obtained according to the Declaration of Helsinki. This study was conducted under the approval of Osaka University Hospital Ethics Committee.

Cell culture

Heparinized bone marrow (BM) aspirate was obtained from iliac BM in surgery under general anaesthesia. Heparinized BM aspirates were plated in tissue culture flasks in culture medium [alpha MEM,

TABLE 1. Clinical and demographic data of patients with RA and OA

	RA patients (n=20)	OA patients (n=26)
Age, mean ± S.D. (range), years	58.9 ± 7.7 (46–81)	73.2 ± 4.4 (46–81)
Duration of RA, mean (range), years	14.3 (8.8–34.0)	–
RF, mean ± S.D., IU/ml	139.5 ± 122.9	–
MMP-3, mean ± S.D., ng/ml	234.5 ± 187.1	–
CRP, mean ± S.D., mg/dl	1.84 ± 1.73	–
DAS28, mean ± S.D., score	4.14 ± 1.03	–
High severity in DAS28 (>5.1), n (%)	5 (25.0)	–
Moderate severity in DAS28 (3.2–5.1), n (%)	13 (65.0)	–
Low severity in DAS28 (<3.2), n (%)	2 (10)	–
Glucocorticoid use, n (%)	15 (75.0)	–
Dosage of glucocorticoid, mean (range), mg/day	5.93 (4–10)	–
DMARD use (including MTX), n (%)	17 (85.0)	–
MTX use, n (%)	11 (55.0)	–
Other DMARD use, n (%)	9 (45.0)	–
Dosage of MTX, mean (range), mg/week	5.64 (2–8)	–

[1]Department of Orthopedics and [2]Department of Clinical Gene Therapy, Osaka University Graduate School of Medicine, Osaka, Japan.

Submitted 17 July 2008; revised version accepted 5 February 2009.

Correspondence to: Tetsuya Tomita, Department of Orthopedics, Osaka University Graduate School of Medicine, 2-2 Yamadaoka, Suita, Osaka, 565-0871, Japan. E-mail: tomita@ort.med.osaka-u.ac.jp

Invitrogen, Carlsbad, CA, USA; 15% fetal bovine serum (FBS), Hyclone Laboratories, Logan, UT, USA; 100 U/ml penicillin and 100 μg/ml streptomycin, Invitrogen]. Cells were incubated at 37°C in a humidified atmosphere of 5% CO_2, and medium was changed every other day. In the control group, cells were incubated in culture medium with 10 mM β-glycerophosphate (bGp) (Calbiochem, San Diego, CA, USA). In the differentiation group, cells were incubated in the culture medium with 10 mM bGp, 100 nM dexamethasone (dex) (Sigma, St Louis, MO, USA) and 82 μg/ml ascorbic acid (Wako Pure Chemicals, Osaka, Japan).

Passage 1 adherent cells were used for flow cytometry. Passage 2 adherent cells were used for ALP staining and activity, Alizarin Red S assay and real-time PCR.

Flow cytometry

Cells were detached with 0.25% trypsin/2 mM EDTA (Invitrogen), washed with FACS buffer [phosphate-buffered saline (PBS), 3% FBS, 0.1% NaN_3], and resuspended in 50 μl FACS buffer. The cells were incubated with 10 μl antibody at 4°C in the dark. After 1 h, the cells were washed with FACS buffer and resuspended in 500 μl FACS buffer. FITC-coupled antibodies against CD14, CD34 (Becton Dickinson, San Jose, CA, USA) and CD105 (R&D Systems, Minneapolis, MN, USA) and phycoerythrin (PE)-coupled antibodies against CD29 and CD45 (Becton Dickinson) were used for analysis. As an isotype control, FITC- or PE-coupled nonspecific mouse IgG (Becton Dickinson) was substituted for primary antibody.

In each analysis, cell fluorescence was evaluated using a FACSCalibur instrument (Becton Dickinson) and data were analysed using Cellquest software (Becton Dickinson). Results were expressed as mean percentage of total positive cells.

Colony-forming assay

Mononuclear cells (MNCs) were separated by Ficoll-Paque Plus (Amersham Biosciences, Stockholm, Sweden) density gradient centrifugation from heparinzed BM aspirates. MNCs from OA and RA ($n=8$, respectively) were recovered from the buffy coat and washed twice with ice-cold PBS. MNCs were plated at a density of 1×10^6 cells/dish in 10-cm culture dishes and incubated in culture medium. Medium was changed every other day. After 2 weeks, ALP staining was performed as described below and these colony-forming units (CFU-ALPs) were counted as ALP-positive colonies. The plates were subsequently stained with crystal violet (Wako Pure Chemicals) and the fibroblasts CFU (CFU-F) were counted as crystal violet-positive colonies. The number of colonies larger than 5 mm was counted in CFU-F and CFU-ALP samples. The ratio of CFU-ALP to CFU-F was calculated in each sample.

ALP staining and activity

Cells were plated at a density of 1×10^4 cells/well in 24-well plates. Cells were divided into the control and the differentiation groups (OA, $n=13$; RA, $n=10$). After 2 weeks, for ALP staining, cells were washed with PBS and fixed with 4% paraformaldehyde for 10 min at 4°C. Cells were washed with 0.056 M 2-amino-2-methylpropanol (AMP; Sigma) buffer and stained by adding substrate solution (0.5 mg naphthol AS-MX phosphate and 0.5 mg Fast Red Violet LB salt/ml 0.056 M AMP buffer), and the reaction was stopped with TE buffer. For ALP activity, cells were washed with PBS and incubated with NP-40 lysis buffer (0.2% NP-40, 50 mM Tris–HCl, 1 mM $MgCl_2$, pH 8.0) for 5 min. Cells were harvested and sonicated. ALP activity was then measured with a commercial Alkaline Phospha B test kit (Wako Pure Chemicals) according to the manufacturer's protocol. In all samples, measurements were performed at least in triplicate and data were calibrated by DNA quantity using a DNeasy Tissue Kit (Qiagen, Valencia, CA, USA).

Alizarin Red S staining and mineralization assay

Cells were incubated by the same method as used for measuring ALP activity (OA, $n=8$; RA, $n=7$). After 3 weeks, cells were washed and fixed with 4% paraformaldehyde for 10 min at 4°C. Cells were washed with PBS and stained with 1% Alizarin Red S solution for 1 h. Then cells were washed with distilled water and incubated with 100 mM cetyl pyridium chloride with shaking on a plate rotator [21]. The extracted supernatant was collected and the optical density was measured at a wavelength of 570 nm against a reference wavelength of 620 nm. In each sample, measurements were performed at least in triplicate and data were calibrated by DNA quantity using a DNeasy Tissue Kit.

RNA extraction

Cells were plated at a density of 2.5×10^5 cells/dish in 10-cm culture dishes and incubated in culture medium with 10 mM bGp, 100 nM dex and 82 μg/ml ascorbic acid (OA, $n=8$; RA, $n=7$). After 2 and 3 weeks, total RNA was extracted by TRIzol reagent (Invitrogen) according to the manufacturer's protocol.

Real time RT-PCR analysis

The cDNA was synthesized from 1 μg of total RNA with a high capacity cDNA archive kit (Applied Biosystems, Foster City, CA, USA). Taqman quantitative real-time PCR amplification was performed in triplicate in 384-well optical plates on the ABI Prism 7700 Sequence Detection System (Applied Biosystems) at 50°C for 2 min and 95°C for 10 min, followed by 40 cycles of 95°C for 15 s and 60°C for 1 min. A threshold cycle (Ct value) was obtained from each amplification curve using software (Applied Biosystems). Data were expressed as fold changes using the $\Delta\Delta$Ct method as described in the manufacturer's guidelines (Applied Biosystems). A ΔCt value was first calculated by subtracting the Ct values for 18S ribosomal RNA from the Ct values from each sample. A $\Delta\Delta$Ct value was calculated by subtracting the ΔCt value of the lowest samples from each group. Fold changes were determined by raising two to the $\Delta\Delta$Ct power. Taqman Gene Expression Assays for pre-made Taqman probe and primer sets (Applied Biosystems) were used for real-time PCR [Primers: ALP, Hs00758162_m1; bone sialoprotein (BSP), Hs00173720_m1; type 1A collagen (COL1A), Hs00164004_m1; osteocalcin (OC), Hs01587813_g1; osteopontin (OPN), Hs00167093_m1; Runt-related transcriptional factor 2 (Runx2), Hs00231692_m1].

Statistical analysis

Data were expressed as mean ± S.D. The Mann–Whitney U-test was used for statistical analysis. A P-value <0.05 was considered to be statistically significant.

Results

Flow cytometry

To clarify whether the content of cells was identical between OA and RA and whether the cells were hMSCs, the phenotype of cells was analysed by flow cytometry.

The results of CD14, CD34 and CD45 were almost completely negative (Fig. 1A–C) and the results of CD29 and 105 were positive in both OA and RA samples (Fig. 1D and E). Mean percentage in CD14, CD34 and CD45 was low (CD14: 1.43 ± 0.40% in OA and 1.1 ± 0.21% in RA; CD34: 0.74 ± 0.09% in OA and 0.89 ± 0.03% in RA; CD45: 1.08 ± 0.28% in OA and 1.15 ± 0.16% in RA) and mean percentage in CD29 and CD105 was high (CD29: 95.36 ± 1.40% in OA and 97.56 ± 1.95% in RA; CD105: 96.83 ± 4.79% in OA and 96.01 ± 6.51% in RA) (Fig. 1F).

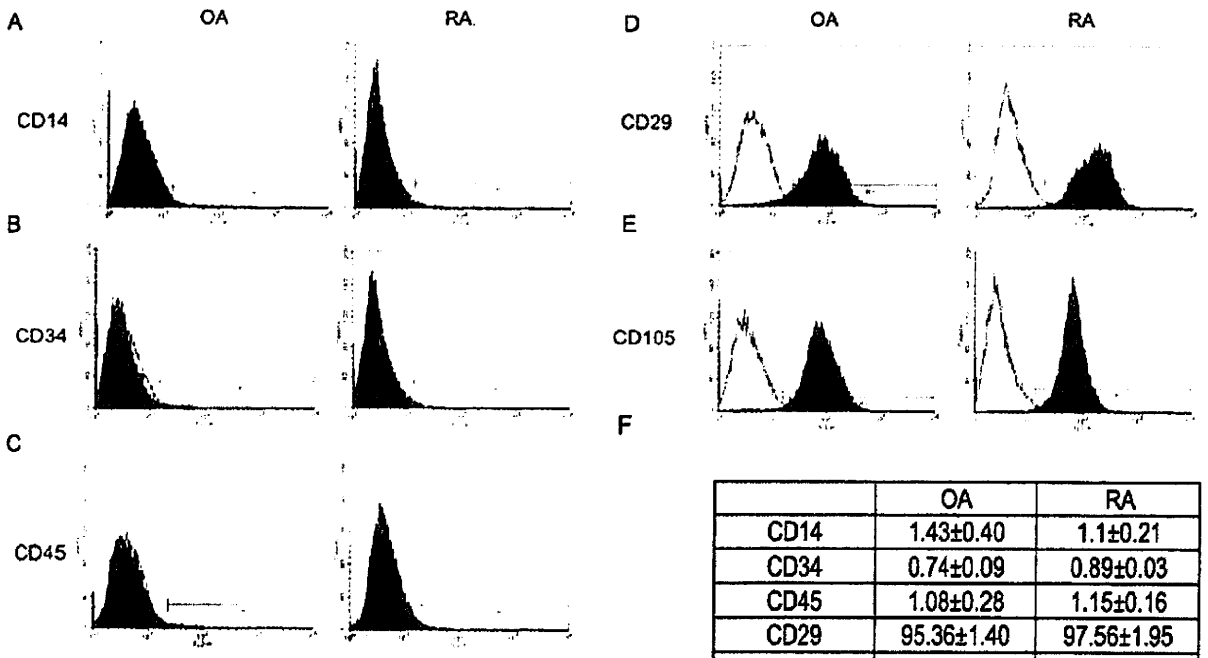

	OA	RA
CD14	1.43±0.40	1.1±0.21
CD34	0.74±0.09	0.89±0.03
CD45	1.08±0.28	1.15±0.16
CD29	95.36±1.40	97.56±1.95
CD105	96.83±4.79	96.01±6.51

Fig. 1. The phenotype of cells in OA and RA. The phenotype of passage 1 cells was analysed by flow cytometry in OA and RA. The results of haematopoietic markers CD14, CD34 and CD45 had almost completely negative expression (A, B, C) and the results of the representative hMSCs markers CD29 and CD105 had positive expression (D, E). The mean percentage of all positive cells from three independent experiments is shown (F).

Colony-forming assay

To examine whether the colony-forming ability of MNCs showed a difference between OA and RA, a colony-forming assay was performed. In CFU-F, the number of positive colonies was 52.1 ± 30.5 in OA and 44.2 ± 20.8 in RA ($P = 0.713$). In CFU-ALP, the number of positive colonies was 39.4 ± 24.3 in OA and 30.6 ± 13.4 in RA ($P = 0.400$) (Fig. 2A). The ratio of CFU-ALP to CFU-F was $75.1 \pm 16.2\%$ in OA and $74.9 \pm 21.9\%$ in RA ($P = 0.793$) (Fig. 2B). There was no significant difference in CFU-F and CFU-ALP and the ratio of CFU-ALP to CFU-F between OA and RA.

ALP staining and activity

To examine how hMSCs are differentiated into osteoblastic cells and produce bone matrix protein, ALP staining and activity were performed. In ALP staining, cells were strongly positive in the differentiation group (Fig. 3A). In ALP activity, mean value was 100.2 ± 54.7 IU/l/μg in OA and 72.6 ± 32.3 IU/l/μg in RA in the control group and 266.8 ± 177.8 IU/l/μg in OA and 307.3 ± 188.1 IU/l/μg in RA in the differentiation group (Fig. 3B). There was no significant difference between OA and RA ($P = 0.137$ in the control group and $P = 0.664$ in the differentiation group).

Alizarin Red S staining and mineralization assay

Alizarin Red S assay expresses calcium deposition of cells and indicates the extent of mineralization. In Alizarin Red S staining, cells were rarely positive in the control group and were strongly positive in the differentiation group (Fig. 4A).

In the Alizarin Red S mineralization assay, the mean value is 0.044 ± 0.023 U/μg in OA and 0.059 ± 0.06 U/μg in RA in the control group and 0.388 ± 0.212 U/μg in OA and 0.227 ± 0.165 U/μg in RA in the differentiation group. There was no significant difference between OA and RA ($P = 0.817$ in the control, $P = 0.094$ in differentiation) (Fig. 4B).

Real-time RT-PCR

To examine the gene expression of cells at the stages of production of bone matrix protein and mineralization in the pathway differentiating hMSCs into osteoblasts, real-time PCR was performed. Gene expression of ALP, BSP, COL1A, OPN, OC and Runx2 mRNA was evaluated by real-time PCR (Fig. 5). Gene expression of ALP, OPN and COL1A at 2 and 3 weeks showed no significant difference between OA and RA. At 3 weeks, gene expression of BSP, OC and Runx2 was significantly higher than at 2 weeks but showed no significant difference between OA and RA. In OA, gene expression of Runx2at 3 weeks was significantly higher than that at 2 weeks. In RA, gene expressions of BSP, OC and Runx2 at 3 weeks were significantly higher than at 2 weeks.

Discussion

In OA and RA, the haematopoietic cell surface antigens such as CD14, CD34 and CD45 were almost completely negatively expressed and the representative hMSC cell surface antigens such as CD29 and CD105 were positively expressed in flow cytometry analysis. These results indicate that the content of cells was identical in OA and RA and the phenotype of cells is thought to be hMSCs [22–24].

In a previous study, it was suggested that the absolute number of MNCs in iliac BM was increased in patients with RA and the ratio of each MNC fraction in iliac BM showed no significant difference between patients with RA compared with the non-RA controls [25]. In this study, the result of colony-forming assay showed no significant difference between OA and RA. This result suggests that the content of MNCs and the ratio of cells in RA, which are differentiated into osteoblastic cells, were not different from those in OA and this is consistent with the result of the previous study.

ALP is an early marker of osteoblast differentiation. COL1A and OPN play an important role for bone formation as bone

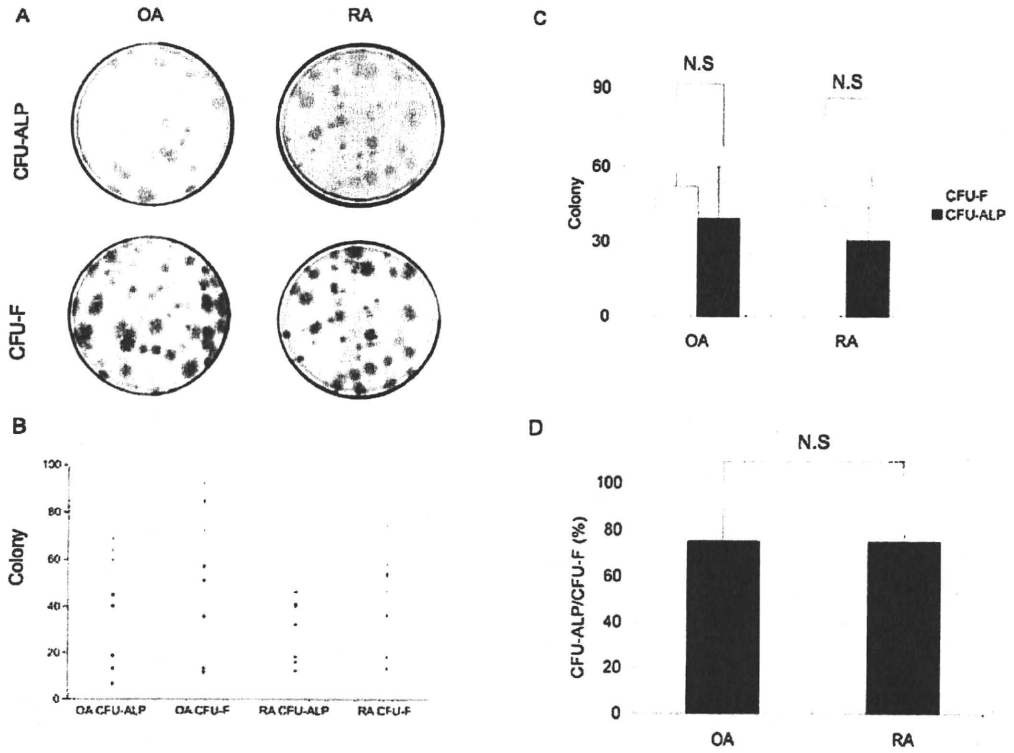

FIG. 2. CFU assay. Mononuclear cells were incubated in culture medium for 2 weeks. In CFU-F, colonies were stained with crystal violet and in CFU-ALP colonies were stained with ALP. The number of colonies with the diameter >5 mm was counted. ALP staining and subsequent crystal violet staining in OA and RA are shown (**A**). The result of CFU-ALP indicated that ALP activity was recognized both in OA and RA. The number of colonies of CFU-F and CFU-ALP in OA and RA was displayed with single dots (**B**) and columns with S.D.-values (**C**). The number of colonies of CFU-F and CFU-ALP showed no significant difference between OA and RA. The ratio of CFU-ALP to CFU-F showed no significant difference between OA and RA (**D**).

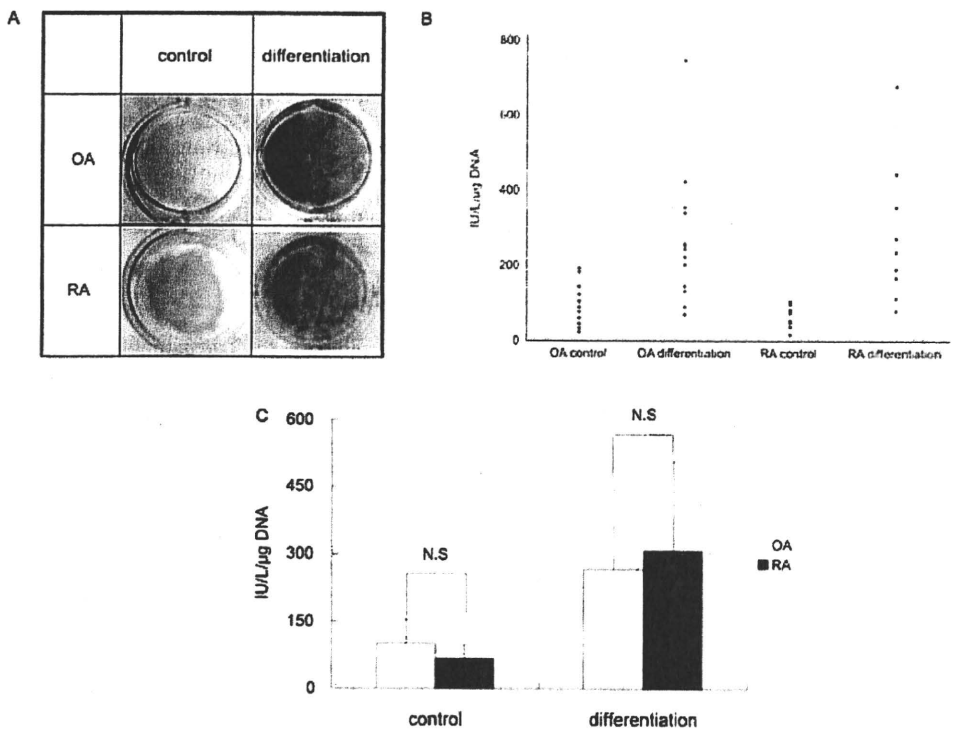

FIG. 3. ALP staining and activity. After incubation for 2 weeks, ALP staining was performed (**A**) and ALP activity was measured by the pNp method. The result of ALP activity in the control and differentiation group both in OA and RA was displayed with single dots (**B**) and with columns and S.D.-values (**C**). ALP activity increased significantly in the differentiation group compared with the activity in the control group in both OA and RA. There was no significant difference between OA and RA in the control and differentiation groups. All samples were performed in triplicate and data were calibrated by DNA quantity.

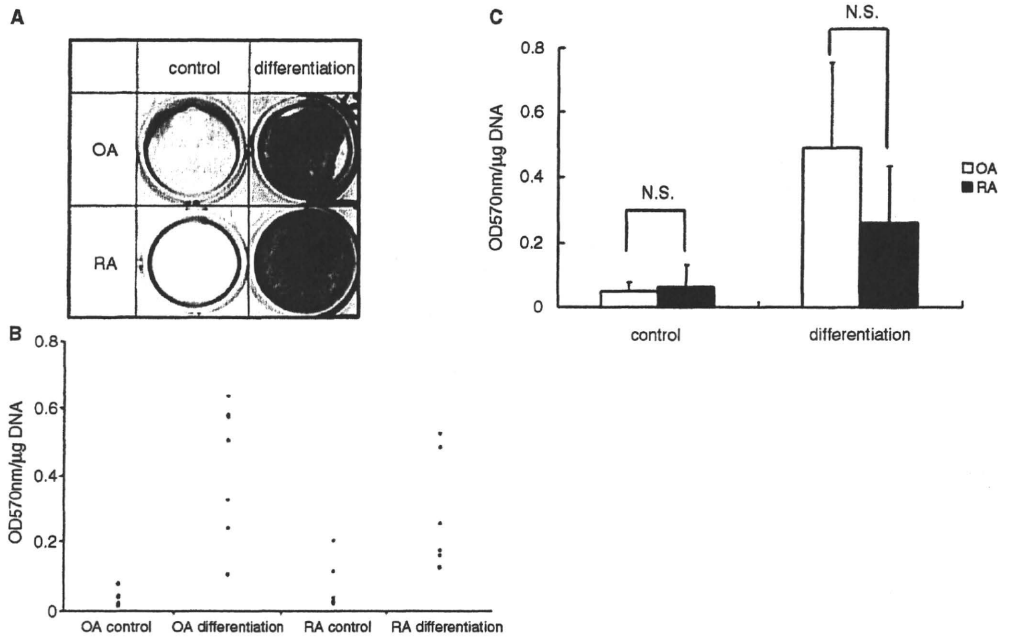

FIG. 4. Alizarin Red S staining and quantitative measuring of mineralization. After incubation for 3 weeks, Alizarin Red S staining was performed (**A**). Quantitative measuring of mineralization was measured by optical density of extracted supernatant at the wavelength of 570 nm. The result of Alizarin Red S mineralization assay in the control and differentiation group both in OA and RA was displayed with single dots (**B**) and with columns and S.D.-values (**C**). The result of the Alizarin Red S mineralization assay increased significantly in the differentiation group compared with that in the control group both in OA and RA. There were no significant differences in the control and differentiation groups between OA and RA. All samples were performed in triplicate and the data were calibrated by DNA quantity.

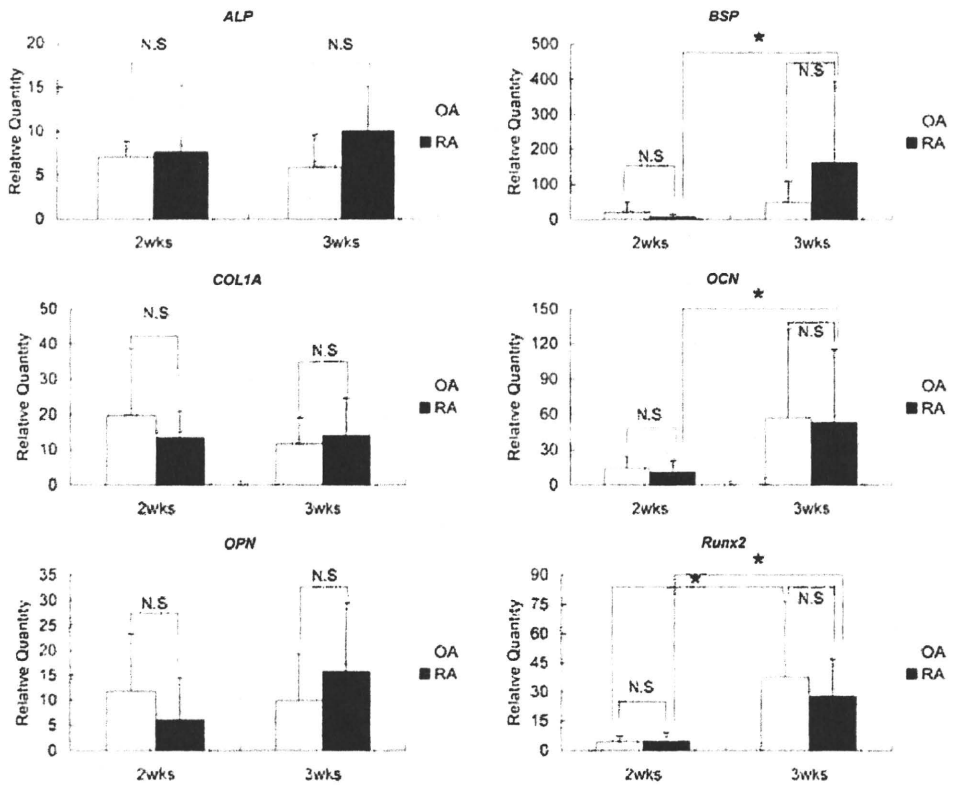

FIG. 5. Real-time PCR analysis. Cells were cultured with bGP, ascorbic acid and dex for 2 and 3 weeks. Real-time PCR was performed and analysed with the $\Delta\Delta$Ct method. The r18s RNA was used as an endogenous control. Gene expressions of ALP, BSP, COL1A, OC, OPN and Runx2 were evaluated. Gene expressions of ALP, COL1A and osteopontin were recognized in both OA and RA at 2 and 3 weeks. In RA, gene expressions of BSP, OC and Runx2 at 3 weeks were significantly higher than those at 2 weeks, and in OA, gene expression of Runx2 at 3 weeks was significantly higher than at 2 weeks. At 2 and 3 weeks, there were no significant differences in gene expressions between OA and RA. All samples were performed in triplicate. Relative quantity data were expressed as mean $\pm$ S.D. ($^*P < 0.05$).

matrix protein. The results of ALP activity and gene expressions of ALP, COL1A and OPN showed no significant difference between OA and RA.

Hydroxyl apatite calcium is formed by a stimulus secreted by osteoblastic cells and mineralization of bone tissue is promoted. BSP and OC are late markers of osteoblast differentiation at the mineralization stage and Alizarin Red S staining expresses the deposition of calcium in cells. In RA samples, gene expressions of BSP and OC at 3 weeks were significantly higher than those at 2 weeks. These results of Alizarin Red S and gene expressions of BSP and OC indicated that hMSCs from patients with RA could be prompted to react by the stimulus and that the function of mineralization of hMSCs in RA was maintained and was almost identical with that in OA.

It was demonstrated that Runx2 is essential for osteoblastic differentiation and promotes gene expression of BSP, OPN and OC, which play roles for differentiating hMSCs into osteoblastic cells [26, 27]. Gene expression of Runx2 showed no significant difference between OA and RA. In both OA and RA, gene expression of Runx2at 3 weeks was significantly higher than those at 2 weeks. These results of this study demonstrate that the function of osteoblastic differentiation of hMSCs shows no significant difference at the stages of production of bone matrix protein and mineralization between OA and RA. It was demonstrated that TNF-α suppressed osteoblast differentiation by suppressing the function of Runx2 *in vitro* [28, 29]. In this study, gene expression in RA was not significantly different from that in OA. The effect of inflammatory cytokines remained unclear and it needs to be further evaluated.

In the present study, there were several limitations. The mean age of patients with OA was higher than that of patients with RA and these groups could not be age matched. We obtained most samples at total knee arthroplasty, which may explain the age difference. We obtained hMSCs from patients with OA and RA in surgery and we could not obtain hMSCs from healthy donors. Therefore, we used hMSCs from patients with OA as a control.

RA is a heterogeneous disease and the backgrounds of patients with RA vary. It was demonstrated that patients with RA are characteristic for general osteoporosis and periarticular bone fragility. Although the main cause of general osteoporosis in RA still remains unclear, it was suggested that the disease activity, immobility and disease duration were associated with reduced bone mass in previous studies [30–32]. In this study, mean DAS28 score was 4.14 and mean CRP was 1.84 mg/dl. These results suggest that the disease activity of patients with RA in this study was moderate and this is because mean duration of disease is relatively longer and treated by appropriate medication.

Most patients with RA in this study have taken steroids. It was suggested that the daily oral and cumulative doses of steroid influenced general osteoporosis in RA [3].

In this study, the mean duration of disease was 14.3 years, which is a relatively longer period, and the mean oral steroid dose was 5.93 mg, which seems to be relatively low. The function of osteoblastic differentiation in RA seems not to be attenuated and the effect of steroid in RA remains unclear. It was demonstrated that relatively low oral dose of MTX did not influence BMD in patients with RA [33, 34]. In this study, mean oral MTX dose was 5. 64 mg/week and orally taken MTX seemed not to affect osteoblastic differentiation. These results were consistent with previous results.

The function of osteoblastic cells in patients with OA and RA was previously evaluated [35]. In this previous study, osteoblastic cells were taken from periarticular bone and the cellular activity and senescence were evaluated. In the present study, we obtained hMSCs from iliac BM and the function of differentiation of hMSCs in patients with RA was evaluated. The previous study suggested the functional potential of MSCs derived from OA and RA especially in cartilage tissue engineering and the possibility of therapeutic application [24]. The present study is the first report to evaluate the function of osteoblastic differentiation of hMSCs from patients with RA.

Although samples from patients with RA were different individually and the results varied widely, the results of this study suggested that hMSCs from patients with RA can be prompted to react by the stimulus of osteoblastic differentiation and maintain the function of osteoblastic differentiation.

Conclusion

In conclusion, we evaluated the function of osteoblastic differentiation of hMSCs at the stages of production of bone matrix protein and mineralization in the present study. The function of osteoblastic differentiation showed no significant difference between OA and RA.

Rheumatology key messages

- hMSCs from patients with RA maintain the function of osteoblastic differentiation.
- The osteoblastic differentiation function of hMSCs derived from RA is equivalent to hMSCs derived from OA.

Acknowledgements

Funding: This work was supported by a grant from Grant-in-Aid for Scientific Research (B) from the Ministry of Education, Culture, Sports, Science and Technology of the Japanese government, and a Grant-in-Aid from Organization for Pharmaceutical Safety and Research.

Disclosure statement: The authors have declared no conflicts of interest.

References

1 Feldmann M, Brennan FM, Maini RN. Rheumatoid arthritis. Cell 1996;85:307–10.
2 Gough AK, Lilley J, Eyre S, Holder RL, Emery P. Generalised bone loss in patients with early rheumatoid arthritis. Lancet 1994;344:23–7.
3 Kroot EJ, Nieuwenhuizen MG, de Waal Malefijt MC, van Riel PL, Pasker-de Jong PC, Laan RF. Change in bone mineral density in patients with rheumatoid arthritis during the first decade of the disease. Arthritis Rheum 2001;44:1254–60.
4 Cooper C, Coupland C, Mitchell M. Rheumatoid arthritis, corticosteroid therapy and hip fracture. Ann Rheum Dis 1995;54:49–52.
5 Hirayama T, Danks L, Sabokbar A, Athanasou NA. Osteoclast formation and activity in the pathogenesis of osteoporosis in rheumatoid arthritis. Rheumatology 2002;41:1232–9.
6 van Staa TP, Geusens P, Bijlsma JW, Leufkens HG, Cooper C. Clinical assessment of the long-term risk of fracture in patients with rheumatoid arthritis. Arthritis Rheum 2006;54:3104–12.
7 Romas E, Gillespie MT, Martin TJ. Involvement of receptor activator of NFkappaB ligand and tumor necrosis factor-alpha in bone destruction in rheumatoid arthritis. Bone 2002;30:340–6.
8 Udagawa N, Kotake S, Kamatani N, Takahashi N, Suda T. The molecular mechanism of osteoclastogenesis in rheumatoid arthritis. Arthritis Res 2002;4:281–9.
9 Goldring SR. Pathogenesis of bone and cartilage destruction in rheumatoid arthritis. Rheumatology 2003;42(Suppl. 2):ii11–6.
10 Strand V, Kavanaugh AF. The role of interleukin-1 in bone resorption in rheumatoid arthritis. Rheumatology 2004;43(Suppl. 3):iii10–6.
11 Erlebacher A, Filvaroff EH, Gitelman SE, Derynck R. Toward a molecular understanding of skeletal development. Cell 1995;80:371–8.
12 Boyle WJ, Simonet WS, Lacey DL. Osteoclast differentiation and activation. Nature 2003;423:337–42.
13 Zaidi M. Skeletal remodeling in health and disease. Nat Med 2007;13:791–801.
14 Compston JE, Vedi S, Croucher PI, Garrahan NJ, O'Sullivan MM. Bone turnover in non-steroid treated rheumatoid arthritis. Ann Rheum Dis 1994;53:163–6.
15 Hall GM, Spector TD, Delmas PD. Markers of bone metabolism in postmenopausal women with rheumatoid arthritis. Effects of corticosteroids and hormone replacement therapy. Arthritis Rheum 1995;38:902–6.
16 Garnero P, Jouvenne P, Buchs N, Delmas PD, Miossec P. Uncoupling of bone metabolism in rheumatoid arthritis patients with or without joint destruction: assessment with serum type I collagen breakdown products. Bone 1999;24:381–5.
17 Pittenger MF, Mackay AM, Beck SC *et al.* Multilineage potential of adult human mesenchymal stem cells. Science 1999;284:143–7.
18 Komori T. Regulation of osteoblast differentiation by transcription factors. J Cell Biochem 2006;99:1233–9.

19 Arnett FC, Edworthy SM, Bloch DA *et al.* The American Rheumatism Association 1987 revised criteria for the classification of rheumatoid arthritis. Arthritis Rheum 1988;31:315–24.
20 Kellgren JH, Lawrence JS. Radiological assessment of osteo-arthrosis. Ann Rheum Dis 1957;16:494–502.
21 Gregory CA, Gunn WG, Peister A, Prockop DJ. An alizarin red-based assay of mineralization by adherent cells in culture: comparison with cetylpyridinium chloride extraction. Anal Biochem 2004;329:77–84.
22 Conget PA, Minguell JJ. Phenotypical and functional properties of human bone marrow mesenchymal progenitor cells. J Cell Physiol 1999;181:67–73.
23 Lee RH, Kim B, Choi I *et al.* Characterization and expression analysis of mesenchymal stem cells from human bone marrow and adipose tissue. Cell Physiol Biochem 2004;14:311–24.
24 Chen FH, Tuan RS. Mesenchymal stem cells in arthritic diseases. Arthritis Res Ther 2008;10:223.
25 Tomita T, Kashiwagi N, Shimaoka Y *et al.* Phenotypic characteristics of bone marrow cells in patients with rheumatoid arthritis. J Rheum 1994;21:1608–14.
26 Komori T, Yagi H, Nomura S *et al.* Targeted disruption of cbfa1 results in a complete lack of bone formation owing to maturational arrest of osteoblasts. Cell 1997;89:755–64.
27 Ducy P, Zhang R, Geoffroy V, Ridall AL, Karsenty G. Osf2/cbfa1: a transcriptional activator of osteoblast differentiation. Cell 1997;89:747–54.
28 Gilbert L, He X, Farmer P *et al.* Inhibition of osteoblast differentiation by tumor necrosis factor-alpha. Endocrinology 2000;141:3956–64.
29 Gilbert L, He X, Farmer P *et al.* Expression of the osteoblast differentiation factor Runx2 (cbfa1/aml3/pebp2alpha a) is inhibited by tumor necrosis factor-alpha. J Biol Chem 2002;277:2695–701.
30 Laan RF, Buijs WC, Verbeek AL *et al.* Bone mineral density in patients with recent onset rheumatoid arthritis: influence of disease activity and functional capacity. Ann Rheum Dis 1993;52:21–6.
31 Haugeberg G, Uhlig T, Falch JA, Halse JI, Kvien TK. Bone mineral density and frequency of osteoporosis in female patients with rheumatoid arthritis: results from 394 patients in the Oslo county rheumatoid arthritis register. Arthritis Rheum 2000; 43:522–30.
32 Lodder MC, de Jong Z, Kostense PJ *et al.* Bone mineral density in patients with rheumatoid arthritis: relation between disease severity and low bone mineral density. Ann Rheum Dis 2004;63:1576–80.
33 Minaur NJ, Kounali D, Vedi S, Compston JE, Beresford JN, Bhalla AK. Methotrexate in the treatment of rheumatoid arthritis. II. In vivo effects on bone mineral density. Rheumatology 2002;41:741–9.
34 di Munno O, Mazzantini M, Sinigaglia L *et al.* Effect of low dose methotrexate on bone density in women with rheumatoid arthritis: results from a multicenter cross-sectional study. J Rheumatol 2004;31:1305–9.
35 Yudoh K, Matsuno H, Osada R, Nakazawa F, Katayama R, Kimura T. Decreased cellular activity and replicative capacity of osteoblastic cells isolated from the periarticular bone of rheumatoid arthritis patients compared with osteoarthritis patients. Arthritis Rheum 2000;43:2178–88.

ARTHRITIS & RHEUMATISM
Vol. 60, No. 12, December 2009, pp 3591–3601
DOI 10.1002/art.25020

Specifically Modified Osteopontin in Rheumatoid Arthritis Fibroblast-like Synoviocytes Supports Interaction With B Cells and Enhances Production of Interleukin-6

Yasuhiro Take,[1] Ken Nakata,[1] Jun Hashimoto,[1] Hideki Tsuboi,[2] Norihiro Nishimoto,[3] Takahiro Ochi,[4] and Hideki Yoshikawa[1]

Objective. **Osteopontin (OPN) is expressed by fibroblast-like synoviocytes (FLS) in rheumatoid arthritis (RA), but its pathologic role is still obscure. The present study was undertaken to analyze the role of OPN in RA by focusing on its effects on cell–cell interactions between FLS and B lymphocytes.**

Methods. **FLS obtained from 10 patients with RA and 10 non-RA subjects and a B lymphocyte cell line were studied. The characteristics of OPN expression by FLS were analyzed by Western blotting, immunoprecipitation, and immunofluorescence studies. In cocultures of FLS and B lymphocytes, the effects of OPN on adhesion of B lymphocytes to FLS and the consequent production of interleukin-6 (IL-6) were analyzed in experiments involving overexpression and knockdown of OPN and inhibitory studies with an OPN-blocking antibody. In vivo, the expression of OPN in RA synovium was examined by immunohistochemistry.**

Results. **A specifically modified 75-kd form of OPN was predominantly expressed in RA FLS, and this was associated with expression of >200-kd thrombin-cleaved OPN that was crosslinked with fibronectin and localized on the surface of the FLS. In FLS–B lymphocyte cocultures, 75-kd OPN–positive FLS produced a significantly higher amount of IL-6 than did 75-kd OPN–negative FLS. When the FLS were separated from B lymphocytes or cultured alone, the production of IL-6 was low and was not significantly different between these 2 culture conditions. Moreover, OPN overexpression enhanced production of IL-6 in 75-kd OPN–positive FLS–B lymphocyte cocultures. Addition of the OPN-blocking antibody inhibited the adhesion of B lymphocytes to FLS. Immunohistochemical analyses revealed that localization of IL-6–positive cells coincided with the sites at which OPN and B lymphocytes were colocalized.**

Conclusion. **Specifically modified 75-kd OPN was expressed by RA FLS. This form of OPN affected FLS–B lymphocyte interactions by supporting the adhesion of B lymphocytes to FLS and enhancing the production of IL-6.**

In patients with rheumatoid arthritis (RA), the synovium of the inflamed joints is the site of a chronic inflammatory reaction, in which leukocytes and macrophages infiltrate, synoviocytes proliferate, and several proinflammatory cytokines (especially, interleukin-6 [IL-6] and tumor necrosis factor α), autoantibodies, and immune complexes are produced (1). In this situation, infiltrating leukocytes and proliferating synoviocytes are thought to interact with each other. Accordingly, several in vitro studies have focused on the interaction between fibroblast-like synoviocytes (FLS) and leukocytes by studying the findings in cocultures of these cells (2–7). Coculture of FLS obtained from RA synovium with B lymphocytes causes adhesion of B lymphocytes to FLS, and consequently this interaction supports the survival of B lymphocytes and also enhances the production of cytokines and immunoglobulin (8–12). The former mechanism is dependent on vascular cell adhesion mol-

Supported by Health and Labour Sciences of Japan research grant 200500732A.

[1]Yasuhiro Take, MD, Ken Nakata, MD, PhD, Jun Hashimoto, MD, PhD, Hideki Yoshikawa, MD, PhD: Osaka University, Suita-city, Osaka, Japan; [2]Hideki Tsuboi, MD, PhD: Osaka Rosai Hospital, Sakai-city, Osaka, Japan; [3]Norihiro Nishimoto, MD, PhD: Wakayama Medical University, Wakayama-city, Wakayama, Japan; [4]Takahiro Ochi, MD, PhD: Osaka Police Hospital, Osaka-city, Osaka, Japan.

Address correspondence and reprint requests to Ken Nakata, MD, PhD, Department of Orthopaedics, Osaka University Graduate School of Medicine, 2-2 Yamadaoka, Suita-city, Osaka 565-0871, Japan. E-mail: ken-nakata@umin.ac.jp.

Submitted for publication February 22, 2009; accepted in revised form August 31, 2009.

ecule 1 (VCAM-1) and very late activation antigen 4 (VLA-4) (10), whereas the latter is yet to be determined.

Osteopontin (OPN) is abundant in the bone matrix, where it acts as a bridge between hydroxyapatite and osteoclasts to support bone resorption (13–15). It is also secreted by T lymphocytes and assists in the maturation of B lymphocytes and the migration of macrophages (16–18). These diverse functions are partly explained by the several functional domains of OPN, including integrin-binding, calcium-binding, and heparin-binding sites. Several studies have revealed that the function of OPN depends on posttranslational modifications (19–24). These modifications, which vary between different OPN-expressing cells, consist of phosphorylation at dozens of serine and threonine residues, along with glycosylation (25), sialylation (21), transglutamination (26), and cleavage (27,28). However, the association between the details of posttranslational modification and the function of OPN is still poorly understood.

As for the relationship between OPN and arthritis, OPN-null mice are protected against inflammatory joint destruction in collagen-induced arthritis (29). A blocking antibody directed against the thrombin-cleaved neoepitope of OPN, which cooperates with several integrin receptors as a ligand (30,31), also shows a curative effect on induced arthritis in mice and monkeys (32,33). Indeed, in patients with RA, OPN, especially in the thrombin-cleaved form, is strongly detected in the synovium and synovial fluid of inflamed joints (34–36). In vitro studies on the function of OPN in arthritis have revealed that OPN stimulates the production of several proinflammatory cytokines by mononuclear cells in patients with RA (37), and also that monocytes obtained from mice with induced arthritis show increased migration toward thrombin-cleaved OPN (32). However, these studies were performed using recombinant OPN, which lacks various posttranslational modifications, and thus the posttranslational modification–dependent functions were not taken into account.

Considering these results and the fact that OPN is also strongly expressed in FLS from the RA synovium (35), we hypothesized that RA FLS express a unique form of OPN that acts to stimulate production of cytokines by creating a bridge between FLS and B lymphocytes in cocultures of these cells. The purpose of this study was to analyze the role of OPN in the development of RA, by focusing on the interaction between FLS and B lymphocytes.

PATIENTS AND METHODS

Patients and cell culture. After obtaining the patients' informed consent and securing Institutional Review Board approval, synovial tissue samples were collected from 11 patients with RA, 8 patients with osteoarthritis of the knee, and 2 patients with medial meniscus degeneration who underwent meniscectomy and synovectomy. All of the patients with RA fulfilled the American College of Rheumatology (formerly, the American Rheumatism Association) revised criteria for RA (38). FLS were isolated by enzymatic digestion of the synovial tissue from 10 patients with RA and 10 non-RA subjects, as described previously (9). The FLS were maintained in Dulbecco's modified Eagle's medium (Gibco BRL, Grand Island, NY) containing 10% fetal bovine serum (FBS; Hyclone Laboratories, Logan, UT) and 1% penicillin/streptomycin (Gibco BRL). Cells from passages 4–10 were used for these experiments. A human B cell line, MC/car, was purchased from the American Type Culture Collection (Rockville, MD) and maintained in RPMI 1640 medium (Gibco BRL) containing 10% FBS and 1% penicillin/streptomycin.

For coculture experiments, 4×10^4 FLS were plated in 12-well plates and, on the following day, 3.3×10^5 B lymphocytes were added to each well. To prevent cell–cell contact between FLS and B lymphocytes, a Millicell culture insert with 0.4-μm pores (Millipore, Billerica, MA) was used. After incubation for 48 hours, enzyme immunoassay (EIA) was performed to measure the concentrations of IL-6 and OPN in the culture supernatant using a homogeneous time-resolved fluorescence human IL-6 assay kit (CIS Bio International, Saclay, France) and a human OPN assay kit (IBL Japan, Gunma, Japan).

Protein collection, sodium dodecyl sulfate–polyacrylamide gel electrophoresis (SDS-PAGE), and Western blotting. Total cell lysates of FLS were collected by placing the cells in lysis buffer (10× Cell Lysis Buffer; New England Biolabs, Beverly, MA), using 4×10^4 FLS plated in 12-well plates and grown in normal growth medium; some of the FLS had undergone transfection with small interfering RNA (siRNA) or lentiviral infection. We did not add any other reagent to the lysis buffer, which consisted of Tris HCl buffer with detergent, protease inhibitor (leupeptin), and phosphatase inhibitors (sodium pyrophosphate, β-glycerophosphate, and sodium orthovanadate). After 1 freeze–thaw cycle, samples were centrifuged and the supernatant was collected. An aliquot was obtained for protein quantification with the bicinchoninic acid assay, and the remaining supernatant was boiled in SDS sample buffer. As a control, recombinant human OPN was used.

Surface protein was collected from 1.2×10^6 FLS using a Cell Surface Protein isolation kit (Pierce, Rockford, IL). Equal amounts of each sample were separated by SDS-PAGE, blotted onto a polyvinylidene difluoride membrane (Hybond-P; Amersham, Piscataway, NJ), and blocked with 5% bovine serum albumin (BSA)/Tris buffered saline containing 0.1% Tween 20 (TBST). The membrane was then incubated overnight at 4°C with one of the following primary antibodies: rabbit anti-human OPN antibody (O-17; IBL Japan) or mouse anti-OPN N-Half antibody (34E3; IBL Japan) (each at 2 μg/ml), which detects the thrombin-cleaved neoepitope YGLR, mouse anti–β-actin antibody (AC-15; Sigma, St. Louis,

MO) at 1:10,000, or rabbit antifibronectin antibody (H-300; Santa Cruz Biotechnology, Santa Cruz, CA) at 1:200. Specificity of the 34E3 antibody was confirmed by Western blotting of thrombin-treated recombinant OPN. After reaction with horseradish peroxidase–conjugated anti-rabbit or anti-mouse IgG and enhanced chemiluminescence Western blotting detection reagents (all from Amersham), images of the membrane were captured using a FAS-1000 Lumino Imaging Analyzer (Toyobo, Osaka, Japan).

Immunoprecipitation analysis. Total cell lysates were prepared for immunoprecipitation using RA FLS from a single patient (RA sample 4 in Figure 1A). When the cells had reached 90% confluence, they were collected in a 10-cm dish, and after centrifugation, the resulting supernatant was precleared with ImmunoPure Immobilized Protein A Plus (Pierce), divided into 3 centrifuge tubes, and incubated overnight at 4°C with protein A–Sepharose bound with 10 μg of the anti-OPN antibody (O-17), the antifibronectin antibody, or normal rabbit IgG (Santa Cruz Biotechnology) as a negative control. On the following day, the samples were washed and eluted with SDS sample buffer, and then analyzed by Western blotting.

Immunofluorescence analysis. FLS cultured in Chamber Slides (Nunc, Rochester, NY) were fixed in 4% paraformaldehyde, permeabilized with TBST, blocked with 5% BSA/TBST, and incubated overnight at 4°C with the anti-OPN antibody (O-17) or normal rabbit IgG (Santa Cruz Biotechnology) (each at 2 μg/ml). After the samples were reacted with Alexa Fluor 488–conjugated anti-rabbit IgG at 1:500 (Molecular Probes, Eugene, OR), the fluorescence intensity of the samples was examined under an epifluorescence microscope (Nikon Eclipse 90i; Nikon, Tokyo, Japan).

Transfection with siRNA. Commercially available, predesigned double-stranded RNA (nontargeting siRNA [siCONTROL Pool #1] and siRNA for human secreted phosphoprotein 1 [OPN] and IL-6 [siGENOME SMARTpool siRNA]; Dharmacon, Lafayette, CO) were used for the RNA interference experiments. One microliter of X-TremeGENE reagent (Roche Diagnostic, Penzberg, Germany) and 20 pmoles of the siRNA from either pool were diluted in serum-free medium, and the mixture was then incubated for 15 minutes and added to 4×10^4 FLS in a 12-well plate. Two days after transfection, messenger RNA (mRNA) was collected and reverse-transcribed to first-strand complementary DNA (cDNA) using a high-capacity cDNA reverse transcription kit. Real-time reverse transcription–polymerase chain reaction (PCR) was then performed to evaluate the OPN-knockdown efficacy, using TaqMan gene expression assays (Applied Biosystems, Foster City, CA). Three days after transfection, the cocultures were started.

B lymphocyte adhesion assay. Adhesion of B lymphocytes to FLS was assessed as described previously (11), with some modifications. Briefly, 6.6×10^3 FLS were plated into a 96-well plate. After 3 days, the cells were incubated at 37°C for 2 hours with a polyclonal OPN-neutralizing antibody or normal goat IgG (both from R&D Systems, Minneapolis, MN) at 10 μg/ml. Subsequently, 3.3×10^5 B lymphocytes were added and incubated at 37°C for another 2 hours. B lymphocytes that did not adhere firmly to the FLS were removed by vigorous washing. Three separate fields were viewed under an inverted microscope at a magnification of 100× per well to count the adherent B lymphocytes, with results expressed quantitatively as the mean number of adherent B lymphocytes.

Transglutaminase inhibition. FLS were plated at 4×10^4 cells in 12-well plates, followed by incubation with cystamine sulfate (500 μM) for 2 days to inhibit transglutaminase activity. Subsequently, total cell lysates were collected for further analysis.

Plasmid construction and lentiviral infection. The full-length OPN-coding sequence was amplified by PCR from a human synovial cell cDNA library using the following primers: 5′-CCCTCGAGATGAGAATTGCAGTGATTTGC-3′ (NM_001040058, nt166–186) and 5′-CGGGATCCTTAATTGACCTCAGAAGATGCAC-3′ (NM_001040058, nt1088–1110). The PCR product was digested with *Xho* I and *Bam* HI, and then purified and ligated to pcDNA3.1 (Invitrogen, Carlsbad, CA) for sequencing. The vector was cut with *Pme* I and the OPN insert was obtained by gel extraction/purification, which was then ligated to the lentiviral expression vector pWPI. Lentivirus infection was performed on 4×10^4 FLS in a 12-well plate, as described previously (39,40). Three days after infection, coculture was started for measurement of IL-6 production.

Immunohistochemistry. Specimens of synovial tissue obtained from a patient with RA were fixed in 10% formaldehyde, dehydrated, and embedded in paraffin. Sections of the tissue were cut (4 μm thick) on a microtome, and then were analyzed by immunohistochemistry, as described previously (41), using the following primary antibodies: rabbit anti-OPN antibody (O-17) or normal rabbit IgG at 2 μg/ml, mouse anti-CD79α antibody (JCB117; Nichirei, Tokyo, Japan) at 1:50, normal mouse IgG1 (R&D Systems), and goat anti-human IL-6 antibody or normal goat IgG at 2.5 μg/ml.

Statistical analysis. Results are expressed as the mean ± SD of at least 3 independent experiments, if not specified. For statistical comparison, 2-way factorial analysis of variance (ANOVA) (sometimes followed by a Bonferroni post hoc test) was performed using SPSS software (version 16.0; SPSS, Chicago, IL). *P* values less than 0.05 were considered significant.

RESULTS

Detection of specifically modified 75-kd OPN in all 10 RA FLS and 3 non-RA FLS, in conjunction with significantly higher IL-6 production in FLS–B lymphocyte cocultures. Western blotting of the total cell lysates from FLS, using the antibody for the N-terminus of OPN (O-17), showed several bands at 75 kd and also around 54 kd (Figure 1A), which is a well-known characteristic of OPN (42). Double bands around 54 kd, each at an equal density, were detected in every FLS sample. Recombinant human OPN also migrated at around 54 kd. However, 75-kd OPN was predominantly detected in all 10 RA FLS samples (RA samples 1–10 in Figure 1A)

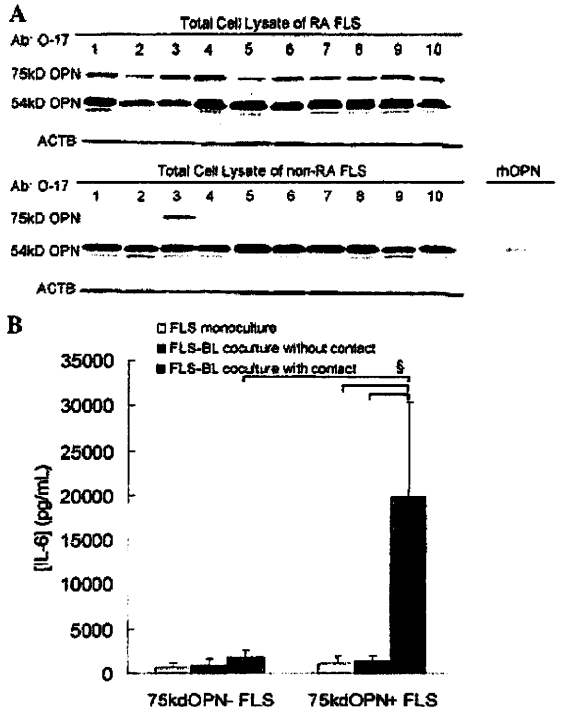

Figure 1. Detection of osteopontin (OPN) and production of interleukin-6 (IL-6) in fibroblast-like synoviocytes (FLS). **A**, Total cell lysates of rheumatoid arthritis (RA) FLS and non-RA FLS (n = 10 samples each) were assessed using Western blotting with an N-terminus antibody (Ab) against OPN (O-17), in comparison with recombinant human OPN (rhOPN); β-actin (ACTB) served as standard. **B**, The concentration of interleukin-6 (IL-6) in the culture supernatants of FLS monocultures, FLS–B lymphocyte (BL) cocultures without contact (separated by a Millicell culture insert), and FLS–B lymphocyte cocultures with contact was evaluated by enzyme immunoassay separately in 75-kd OPN–positive FLS (n = 13) and 75-kd OPN–negative FLS (n = 7). Bars show the mean and SD. § = $P < 0.001$ by Bonferroni *t*-test.

and in only 3 non-RA FLS samples (non-RA samples 3, 8, and 9). Thrombin-cleaved OPN was not detected around the reported molecular weight of 30 kd (43).

EIA analysis of the full-length OPN secreted in the culture supernatant showed that the concentration of OPN was 9–18 ng/ml, and this did not differ between RA and non-RA FLS (results not shown). Since the expression of 75-kd OPN was distinct, FLS were grouped into 75-kd OPN–positive and 75-kd OPN–negative FLS.

Production of IL-6 was evaluated by EIA for determination of the IL-6 concentration in the culture supernatants obtained in several culture conditions with FLS and B lymphocytes. In FLS monoculture (i.e., FLS cultured alone), the mean ± SD IL-6 production by the 75-kd OPN–positive FLS (n = 13) and the 75-kd OPN–negative FLS (n = 7) was 1,113.3 ± 818.9 pg/ml and 643.1 ± 576.5 pg/ml, respectively. In FLS–B lymphocyte cocultures without contact (i.e., FLS cocultured with B lymphocytes, but separated by the Millicell culture insert), the IL-6 levels were 1,363.3 ± 714.6 pg/ml in 75-kd OPN–positive FLS and 902.6 ± 772.5 pg/ml in 75-kd OPN–negative FLS. There were no significant differences in IL-6 production among these 4 groups.

However, in cocultures with contact (i.e., FLS and B lymphocytes cultured in contact with each other), IL-6 production was significantly elevated in 75-kd OPN–positive FLS, and showed a tendency to be elevated, although not to a significant extent, in 75-kd OPN–negative FLS. The IL-6 production by the 13 FLS positive for 75-kd OPN cocultured in contact with B lymphocytes was elevated to 19,928.5 ± 10,351.8 pg/ml, which was significantly higher than that in the other 2 culture conditions ($P < 0.001$, by Bonferroni *t*-test) and significantly higher than that in the 7 FLS negative for 75-kd OPN that were in contact coculture with B lymphocytes (910.9 ± 744.1 pg/ml; $P < 0.001$, by Bonferroni *t*-test) (Figure 1B).

Transfection of the FLS with IL-6 siRNA significantly reduced the levels of IL-6 in the 75-kd OPN–positive FLS that were in contact coculture with B lymphocytes. In contrast, when B lymphocytes were cultured alone, IL-6 was not detected in the culture supernatants (results not shown).

Production of >200-kd thrombin-cleaved OPN in the cell surface protein fraction of 75-kd OPN–positive FLS, and cell membrane distribution of OPN. Analysis of cell surface proteins from FLS, using Western blotting with an antibody against the thrombin-cleaved neoepitope of OPN (34E3), detected the presence of >200-kd OPN in the surface fraction of 75-kd OPN–positive FLS. This band was poorly detected in 75-kd OPN–negative FLS or in the nonsurface fraction of FLS (Figure 2A). A similar result was obtained with the O-17 antibody, but the signals were much weaker (results not shown). As a loading control, Western blotting with the antifibronectin antibody probe was performed. When the anti-OPN antibody O-17 was used to analyze the 75-kd OPN–positive FLS by immunofluorescence assay, the distribution of OPN followed the cell outline, regardless of permeabilization (Figure 2B).

Detection of >200-kd OPN in the immunoprecipitant by antifibronectin antibody, and reduction by transglutaminase inhibitor treatment. According to a previous study, OPN appears at >200 kd when it is

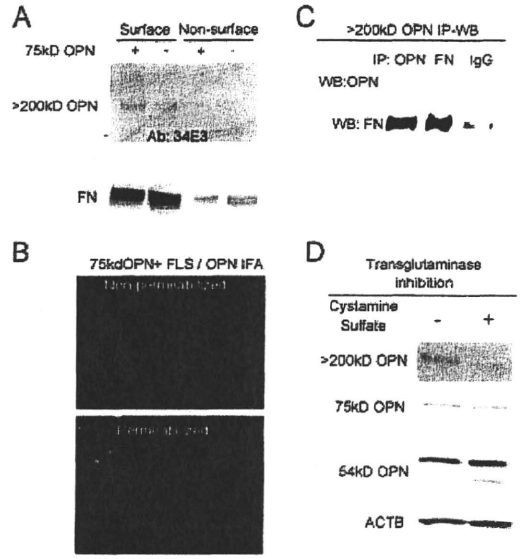

Figure 2. Characteristics of the 75-kd OPN. **A,** Isolation of cell surface proteins was followed by Western blotting with or without the antibody (Ab) directed against the thrombin-cleaved neoepitope of OPN (34E3). The >200-kd form of OPN was detected in the surface protein fraction of 75-kd OPN–positive FLS. Fibronectin (FN) expression was used as the loading control. **B,** Immunofluorescence assay (IFA) was used to assess the expression pattern of OPN on 75-kd OPN–positive FLS stained with OPN antibody O-17, with results showing a distribution of OPN corresponding to the cell outline, regardless of permeabilization. **C,** When >200-kd OPN was further examined by immunoprecipitation–Western blotting (IP-WB), the >200-kd band was detected in the immunoprecipitant of the OPN antibody (O-17) blotted with the FN antibody, and vice versa. Normal rabbit IgG was used as the negative control. **D,** The OPN–positive FLS were treated with or without a transglutaminase inhibitor, cystamine sulfate, and assessed by Western blotting. Expression of >200-kd OPN was reduced by treatment with cystamine sulfate, whereas the expression levels of 75-kd and 54-kd OPN were not altered. See Figure 1 for other definitions.

covalently crosslinked to fibronectin by transglutamination through 2 widely conserved glutamine residues at its N-terminus (26). Therefore, immunoprecipitation of total cell lysates from 75-kd OPN–positive FLS with the anti-OPN or antifibronectin antibody was performed, and this was followed by Western blotting with these antibodies. The >200-kd band was detected when the immunoprecipitant obtained with the antifibronectin antibody was probed by the anti-OPN antibody, and vice versa (Figure 2C). A transglutaminase inhibitor, cystamine sulfate, reduced the expression of >200-kd OPN when the inhibitor was added to the FLS cultures, but did not alter the levels of 75-kd or 54-kd OPN (Figure 2D).

Enhanced IL-6 production by OPN overexpression in 75-kd OPN–positive FLS, but not in 75-kd OPN–negative FLS, in cocultures with B lymphocytes. To elucidate the role of OPN in FLS–B lymphocyte cocultures, gain of function experiments were performed by inducing overexpression of OPN with a lentiviral vector. Western blotting of the cells after lentiviral infection showed that all 75-kd OPN–positive FLS showed up-regulation of the 75-kd, >200-kd, and 54-kd OPN bands, along with an extra band at 50 kd, whereas the 75-kd and >200-kd bands were not up-regulated in any of the 75-kd OPN–negative FLS (Figure 3A).

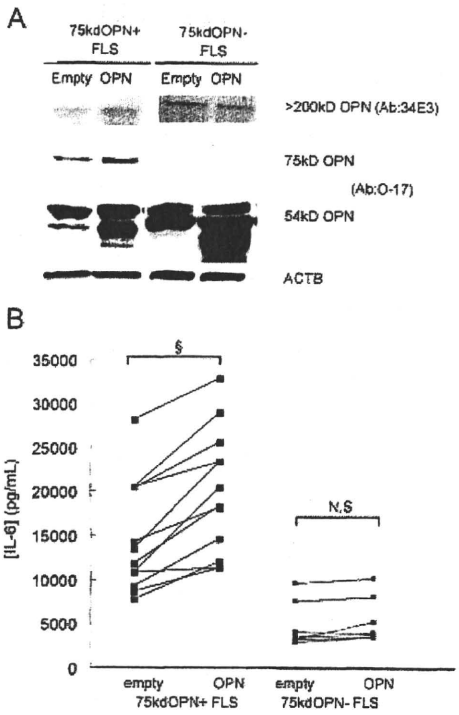

Figure 3. Gain of function experiments, targeting OPN by lentiviral infection with an overexpression vector. **A,** The 75-kd OPN–positive and 75-kd OPN–negative FLS were subjected to lentiviral infection with an empty vector or OPN-overexpressing vector and then assessed by Western blotting. The 54-kd form of OPN, with an extra lower band, showed increased expression in both types of FLS, while >200-kd OPN and 75-kd OPN were increased only in 75-kd OPN–positive FLS. **B,** After lentiviral infection of the FLS and then coculture in contact with B lymphocytes, the IL-6 concentration in the culture supernatant was evaluated. IL-6 levels were significantly increased by OPN overexpression in 75-kd OPN–positive FLS, whereas the levels were not altered in 75-kd OPN–negative FLS. Solid squares show individual FLS samples. § = $P < 0.001$ by 2-factorial analysis of variance. NS = not significant (see Figure 1 for other definitions).

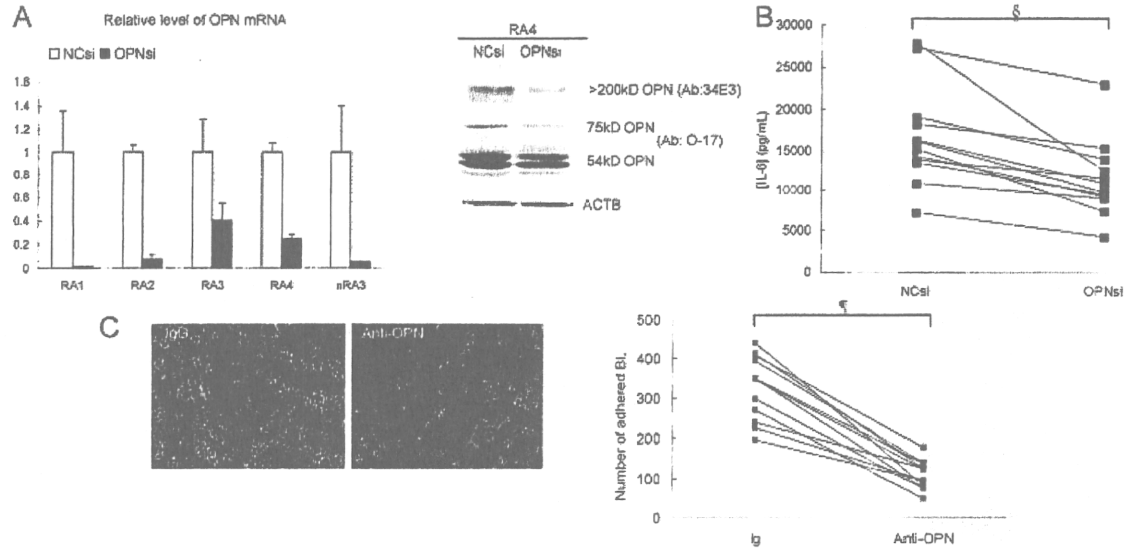

Figure 4. Loss of function experiments, targeting OPN by small interfering RNA (siRNA) (A and B) and a neutralizing antibody (C). A, OPN knockdown in 75-kd OPN–positive FLS by transfection of OPN siRNA (OPNsi) was evaluated by real-time reverse transcription–polymerase chain reaction (left) and by Western blotting (right). Bars show the mean and SD OPN mRNA levels in triplicate experiments with each of 4 RA FLS samples and 1 non-RA (nRA) FLS sample. NCsi = negative control siRNA. B, FLS transfected with negative control siRNA or OPN siRNA were cocultured in contact with B lymphocytes and the IL-6 concentration in the supernatant was evaluated. The IL-6 level was significantly reduced by OPN knockdown. § = $P < 0.001$ by 2-factorial analysis of variance. C, FLS treated with an OPN-neutralizing antibody or class-matched normal IgG were cocultured in contact with B lymphocytes. After removal of nonadherent B lymphocytes by vigorous washing, adherent B lymphocytes were counted in 3 separate fields per well, as viewed under an inverted microscope (left; original magnification × 100). Small round cells are B lymphocytes. The number of adherent B lymphocytes was expressed as the mean (right). Solid squares show individual FLS samples. ¶ = $P < 0.001$ by 2-factorial analysis of variance. See Figure 1 for other definitions.

In addition, all 75-kd OPN–positive FLS showed a significant increase in IL-6 production after OPN overexpression followed by coculture in contact with B lymphocytes, when compared with cells without overexpression ($P < 0.001$ by 2-factorial ANOVA) (Figure 3B). In 75-kd OPN–negative FLS, however, IL-6 production was not altered by overexpression of OPN, which was consistent with the lack of a 75-kd band and the unaltered >200-kd band on Western blotting.

Significant reduction in IL-6 levels following loss of function of OPN in 75-kd OPN–positive FLS, and inhibition of adhesion of B lymphocytes on FLS in cocultures with B lymphocytes. Loss of function experiments were performed using siRNA transfection and an OPN-neutralizing antibody. Transfection of OPN siRNA successfully knocked down OPN expression at the mRNA level as well as at the protein level in all of the 75-kd OPN–positive FLS (Figure 4A). After subsequent coculture of the FLS in contact with B lymphocytes, there was significantly lower IL-6 production by OPN–knocked down FLS compared with that by FLS transfected with nontargeting siRNA ($P < 0.001$ by 2-factorial ANOVA) (Figure 4B).

Adhesion of B lymphocytes to FLS occurred in FLS–B lymphocyte cocultures, as has been reported previously (9,12), but was inhibited by the blocking antibody directed against OPN. The number of B lymphocytes adherent to FLS was significantly reduced by the anti-OPN antibody in all 75-kd OPN–positive FLS ($P < 0.001$ by 2-factorial ANOVA) (Figure 4C).

Detection of IL-6–positive cells in the sublining region of RA synovium, at the site of OPN–B lymphocyte colocalization. Finally, to assess the distribution of OPN, IL-6, and B lymphocytes in the RA synovium, immunohistochemical analyses were carried out using anti–IL-6, anti-OPN, and anti–pan B lymphocyte antigen CD79α antibodies. One of the synovial villi located in the knee joint from an RA patient was studied. As reported previously, OPN was distributed in the fibroblastic cells and the matrix of the synovial lining and sublining regions (34,35). Clusters of B lymphocytes were found in the deeper layers of the synovium as well as in the